Co-registered Topographical, Band Excitation Nanomechanical, and Mass Spectral Imaging Using a Combined Atomic Force Microscopy/Mass Spectrometry Platform

Olga S. Ovchinnikova,*,† Tamin Tai,† Vera Bocharova,‡ Mahmut Baris Okatan,§,∥ Alex Belianinov,§,∥ Vilmos Kertesz,† Stephen Jesse,§,∥ and Gary J. Van Berkel*,†

†Organic and Biological Mass Spectrometry Group, Chemical Sciences Division, Oak Ridge National Laboratory, Oak Ridge, Tennessee 37831-6131, United States, ‡Soft Materials Group, Chemical Sciences Division, Oak Ridge National Laboratory, Oak Ridge, Tennessee 37831-6131-6210 , United States, §Imaging & Nanoscale Characterization Group, Center for Nanophase Materials Sciences, Oak Ridge National Laboratory, Oak Ridge, Tennessee 37831-6487, United States, and ∥Institute for Functional Imaging of Materials, Oak Ridge National Laboratory, Oak Ridge, Tennessee 37831-6487, United States

ABSTRACT The advancement of a hybrid atomic force microscopy/mass spectrometry imaging platform demonstrating the co-registered topographical, band excitation nanomechanical, and mass spectral imaging of a surface using a single instrument is reported. The mass spectrometry-based chemical imaging component of the system utilized nanothermal analysis probes for pyrolytic surface sampling followed by atmospheric pressure chemical ionization of the gas-phase species produced with subsequent mass analysis. The basic instrumental setup and operation are discussed, and the multimodal imaging capability and utility are demonstrated using a phase-separated polystyrene/poly(2-vinylpyridine) polymer blend thin film. The topography and band excitation images showed that the valley and plateau regions of the thin film surface were comprised primarily of one of the two polymers in the blend with the mass spectral chemical image used to definitively identify the polymers at the different locations. Data point pixel size for the topography (390 nm × 390 nm), band excitation (781 nm × 781 nm), and mass spectrometry (690 nm × 500 nm) images was comparable and submicrometer in all three cases, but the data voxel size for each of the three images was dramatically different. The topography image was uniquely a surface measurement, whereas the band excitation image included information from an estimated 20 nm deep into the sample and the mass spectral image from 110 to 140 nm in depth. Because of this dramatic sampling depth variance, some differences in the band excitation and mass spectrometry chemical images were observed and were interpreted to indicate the presence of a buried interface in the sample. The spatial resolution of the chemical image was estimated to be between 1.5 and 2.6 μm, based on the ability to distinguish surface features in that image that were also observed in the other images.

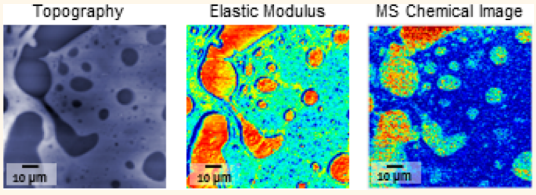

KEYWORDS: atomic force microscopy · mass spectrometry imaging · atmospheric pressure chemical ionization · thermal desorption · band excitation · topography · atmospheric pressure

We recently introduced atmospheric pressure (AP) proximal probe thermal desorption/secondary ionization combined with mass spectrometry (TD/SI-MS) for direct spatially resolved chemical profiling and imaging of surfaces.[1−4] With this surface sampling/ionization and analysis approach, heated probe tips, ranging in size from a few millimeters to 30 nm in close proximity to or in actual contact with a surface, have been used to locally desorb intact molecular species. The desorbed species were then ionized by an AP ionization source such as electrospray ionization (ESI) or atmospheric pressure chemical ionization (APCI) and analyzed using MS.

To push the capabilities of the AP TD/SI-MS approach toward submicrometer spatial spot sampling and imaging resolution, we advanced a hybrid atomic force microscopy (AFM)-ESI or APCI/mass spectrometry system utilizing 30 nm diameter nanothermal analysis (nano-TA) probes for TD surface sampling.[3,4] The heated nano-TA probes are made from a doped single-crystal silicon. The probe tip temperature can be precisely

* Address correspondence to ovchinnikovo@ornl.gov, vanberkelgj@ornl.gov.

Received for review January 29, 2015 and accepted March 10, 2015.

Published online March 18, 2015
10.1021/acsnano.5b00659

controlled over the temperature range 25−1000 °C, using a resistive heater integrated into the cantilever.[5] With this hybrid instrumentation we have been able to achieve co-registered AFM topographical images of surfaces with mass spectral signal from 250 nm spot samples[3] and 2.5 μm × 2.0 μm pixel size mass spectral chemical images.[4] Over a decade ago a similar proximal probe thermal desorption/pyrolysis approach using AFM was demonstrated by Price and co-workers.[6−10] In those experiments material was liberated to the gas phase, captured, and then injected into a gas-chromatograph mass spectrometer (GC/MS) for separation, electron ionization (EI), and mass analysis. More recently, de Vries *et al*. used nano-TA probes to thermally desorb various organic dyes from surfaces using ambient desorption/collection onto a graphite substrate followed by a vacuum laser desorption/resonant two-photon ionization (R2PI) MS analysis.[11] In neither the work of Price or de Vries was mass spectrometry information from more than an individual spot or a series of a few spot samples obtained.

Beyond topographic imaging, scanning probe techniques have found an extremely broad range of applications in probing electrical, magnetic, optical, and mechanical properties on a single system, opening up the possibility of understanding material functionality at their relevant length scales.[12] Therefore, with the goal of creating a system that can better characterize the functionality of a material, we have begun to explore the addition of a nanomechanical imaging mode, *viz*., band excitation (BE), into our hybrid AFM/MS system. Outside of BE, various AFM-based methods for measuring material nanomechanical properties are available. The acquisition of force−distance curves has historically been the method of choice, as they offer fairly easy to interpret information on substrate modulus.[13] Traditionally these methods were very slow and not suitable for mapping. Recent advances have enabled a several hundred times increase in force−distance curve acquisition speeds.[14−16] A remaining drawback for accurate measurements of modulus from force−distance curves is that the stiffness of the cantilever should be close to the stiffness of the tip−surface junction.[17] For most materials this would require a fairly stiff cantilever (on the order of 100 to 1000 N/m). The nano-TA probes typically have a stiffness of around 1 N/m,[18] thus significantly reducing their sensitivity and effectiveness in force−distance-based measurements. Contact resonance-based measurements tend to be very sensitive to nanoscale mechanical properties because they can utilize cantilever resonance to amplified forces at the tip−surface junction, are based on frequency shift information, which is inherently a very sensitive transduction pathway, and are relatively fast because cantilever resonances are typically on the order of 100's of kHz. However, contact resonance methods do require operating at a cantilever resonance. This requires either a feedback loop in the case of dual amplitude resonance tracking (DART),[19] which can be problematic if the resonance frequency changes abruptly during a scan or if the oscillation amplitude becomes too small, or broad-band excitation as in BE, which is not subject to the instabilities of a feedback loop. In addition, nano-TA probes are ideally suited for contact resonance measurements in that they can be used in the Lorentz-force[20] or i-drive[21] configurations so that the actuation force is applied directly at the tip of the cantilever. This configuration is highly preferred over actuation to the base of the cantilever or through the sample as in traditional atomic force acoustic microscopy (AFAM). For these reasons, we chose BE as the most suitable means to acquire nanoscale mechanical measurements quickly and reliably.

While co-registered AFM topographic and mass spectral chemical images of a surface provide more information than either technique alone, as demonstrated by the impetus to combine the two techniques onto one platform,[22−24] the ability to acquire additional complementary chemical or physical information regarding the same surface, within the same instrumentation, might be expected to lead to yet greater understanding.[25−29] Although it is possible to separate the measurements onto separate commercially available platforms, the ability to carry out both physical and chemical characterization on one system allows for inherent co-registration of the acquired data, which minimizes positional uncertainty and image artifacts that arise when trying to combine and overlay data acquired on multiple instruments. Additionally, nano-TA cantilevers are particularly well suited for nanomechanical measurements *via* Lorentz-force actuation, resulting in synergy not only in the data acquired but also in the instrumental setup itself. To acquire a BE image of a surface, the AFM cantilever probe is excited by a waveform of a finite spectral density band centered on the resonance frequency of the probe.[30−32] Typically, shifts in either the contact resonance frequency or the *Q* factor are used to decipher qualitative changes in mechanical properties of the sample; both will shift with changes in the elastic modulus and viscosity.[5,30] Therefore, we are able to perform semiquantitative measurements of the elastic modulus, *i.e*., Young's modulus, based on the measured contact resonance frequency shift. However, due to the only semiquantitative nature of the nanomechanical measurements, and the possibility that very chemically distinct materials have very similar Young's modulus values,[33] the ability to combine nanomechanical imaging, which can identify distinct regions of varying mechanical property, with a chemically specific detection technique such as MS, as well as topographical information, offers the potential to more fully characterize surface structure and chemistry.

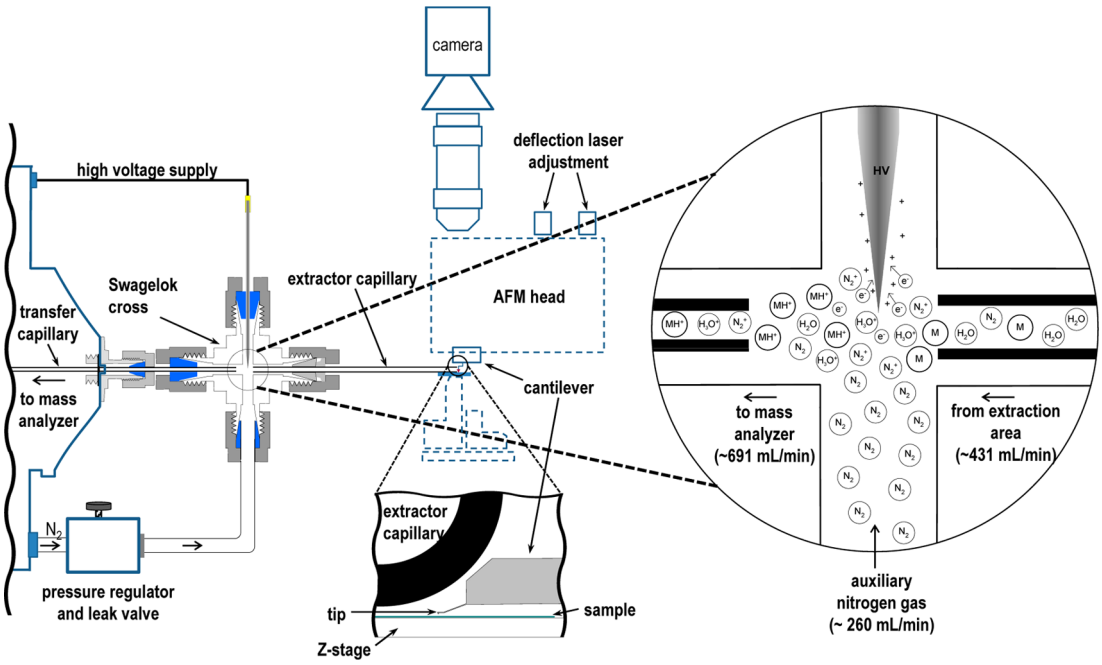

Figure 1. Schematic illustration of the combined AFM/MS experimental setup with an enlarged view showing the details of the inline APCI and ion molecule chemistry and an enlarged view of the AFM nano-TA probe positioned ~0.3 mm away from the sampling capillary.

A relevant system for study is provided by phase-separated thin films. Phase separation in polymer blends is a well-studied topic.[34−37] While there are theoretical and experimental approaches to predict dynamics of bulk phase separation in polymer blends, the behavior of thin film polymer blends is more complicated and, hence, less well understood. Work on thin films of homopolymers has shown that the interface formed between the polymer and the substrate strongly modifies the dynamics of the polymers in the mesoscopic region, resulting in a change of polymer mobility.[34] In thin film multicomponent polymer films, polymer dynamics are further complicated due to the polymer−polymer interactions that often initiate the phase separation on various length scales. Understanding the mechanisms controlling polymer phase separation is highly desirable in practical applications such as organic photovoltaics,[38] where the device efficiency can be enhanced by gaining control of the length scale of phase separation. Therefore, it becomes important to have new experimental insight into the actual phase separation in thin film polymer blends happening at the mesoscale for both fundamental and applied sciences.

In this paper, we demonstrate for the first time the capability to obtain, on the same instrument platform, co-registered AFM-based topographical and BE nanomechanical images as well as mass spectrometry-based chemical images of a sample surface. That capability is demonstrated using a fast-separated polystyrene/poly(2-vinylpyridine) (PS/P2VP) thin film as a model system. Because of the nature of the sample, the nano-TA probes were used to sample from the surface *via* pyrolysis (~450 °C) *versus* simple TD as we have done in the past. The topography and BE images showed that the valley and plateau regions of the thin film surface were comprised primarily of one of the two polymers in the blend, while the mass spectral chemical image was used to definitively identify the polymers at these different locations. Data point pixel size was comparable and submicrometer for all three image types, but voxel size was dramatically different. The topography image was uniquely a surface measurement, whereas the BE and mass spectral images included information from depths of about 20 nm and 110−140 nm into the sample, respectively.

RESULTS

AFM−MS Coupling. We have used two different types of interfaces in our prior work for the coupling of AFM and MS, enabling continuous collection and ionization of material liberated from a surface by the AFM TD process followed by subsequent mass analysis of the ions formed at AP.[3,4] One interface was an in-line ionization "Y" tube inlet design (termed *y*-interface) that used ESI,[3] and the other was a straight line transfer capillary in a modified mass spectrometer ion source using APCI.[4] In the present work, we used an in-line vapor extractor/constant current corona discharge APCI source (Figure 1), which proved to be more effective in our hands for sampling and ionization than either of the other two designs. For select model compounds (*e.g.*, rubrene and pigment yellow 74), the new inline cross interface produced about 5 times

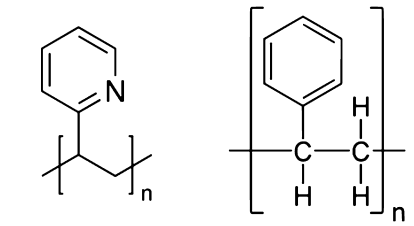

Poly (2-vinylpyridine) P2VP | Polystyrene PS

Scheme 1. Structure of P2VP and PS polymers.

the signal intensity of the former *y*-interface and about 45 times the signal of the modified ion source design (data not shown). Volatilized material was transported by the vacuum pull of the mass spectrometer into the extractor capillary that was positioned within ~300 μm of the AFM probe tip. Reagent ions produced *via* the corona discharge in the center of the interface cross ionized the vapor phase materials drawn into the interface at this point, but ion−molecule chemistry could continue to occur during the transit of ions and neutrals down the transfer capillary toward the vacuum region of the mass spectrometer. The vacuum draw from the mass spectrometer was measured as ~691 mL/min, resulting in a calculated reaction time in the cross center of approximately 0.82 ms. This might be viewed as a minimum reaction time in this system. By adding an auxiliary nitrogen flow into the cross signal levels for compounds relevant to the materials under study (*e.g.*, 2-vinylpyridine) were enhanced. Under optimized conditions, the addition of the auxiliary nitrogen gas slowed the flow through the extractor capillary to ~431 mL/min, effectively extending the minimum reaction time by about a factor of 1.6 times. A reaction time of ten to several hundred milliseconds is typical for most APCI sources.[39] Ambient air (N_2, O_2, and H_2O vapor) was drawn into the source along with the volatilized surface materials so that in positive ion mode the major reagent ions were normally protonated water/water clusters.[39,40] As such, the major ion−molecule reaction with the vapor material sampled was expected to be proton transfer, resulting in the formation of protonated molecules $(M + H)^+$.

AFM-TD/APCI-MS of Polymers. Obtaining a mass spectral-based chemical image from high molecular weight PS and P2VP polymers (Scheme 1) required pyrolysis of the material with the nano-TA probes. The pyrolysis process produced lower mass polymer oligomers in the gas phase that could potentially be ionized and subsequently detected. Pyrolysis of the present polymers was accomplished by heating the nano-TA tips to ~450 °C. However, because of the nature of the APCI process,[39,40] only the products of the P2VP pyrolysis could be detected. The 2-vinylpyridine molecule and this moiety in the low mass oligomers make these species basic enough to be ionized by proton transfer

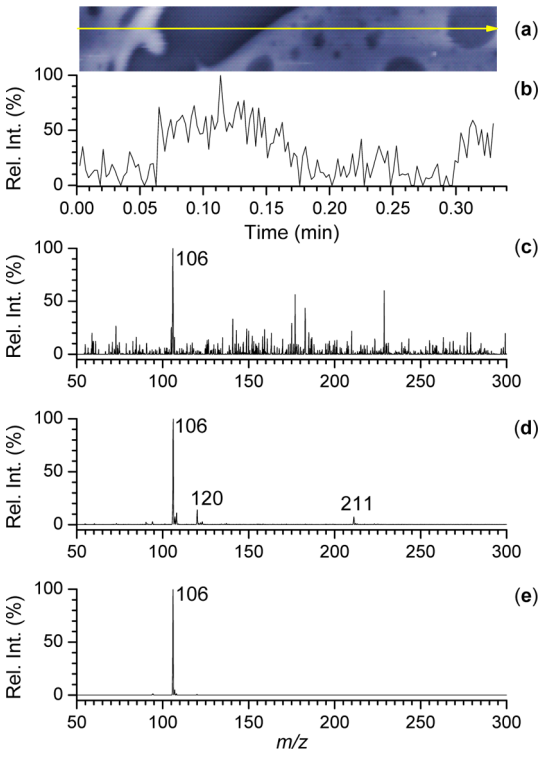

Figure 2. (a) Topographic image of a phase-separated thin film of PS/P2VP showing different domains (yellow arrow indicates a line scan with the AFM probe at ~450 °C). (b) Extracted ion current chronogram for *m/z* 106 obtained during the line scan shown in (a). (c) Background-subtracted full scan positive ion mode mass spectrum obtained by averaging over the 0.07−0.15 min time window in (b). (d) Background-subtracted full scan positive ion mode mass spectrum obtained by spot sampling a P2VP bead with the AFM probe at ~450 °C. (e) Full scan positive ion mode mass spectrum obtained by sampling the headspace vapor of 2-vinylpyridine (105 Da) into the in-line APCI sampling capillary.

with protonated water/water clusters in the APCI source. This was confirmed by sampling a 2-vinylpyridine vapor sample into the APCI region and detection of the protonated molecule, $(M + H)^+$, at *m/z* 106 (see Figure 2e).

Shown in Figure 2a is a rectangular segment from a topographical image of the phase-separated PS/P2VP thin film. Figure 2b is the extracted ion chronogram for *m/z* 106 corresponding to the protonated pyrolysis product 2-vinylpyridine, which was detected during a line scan of the heated nano-TA probe across the surface in the area indicated by the yellow arrow in Figure 2a. During this scan, the heated probe sampled from the surface by pyrolysis created a roughly 500 nm wide by ~100 nm deep trench in the sample. For this reason, the mass spectral chemical image of the surface was rendered using mass spectral data obtained from a series of line scans spaced 500 nm apart (see below). Protonated 2-vinylpyridine (*m/z* 106) was detected in the full scan mass spectrum when the probe sampled from a P2VP-containing region (Figure 2c). Figure 2c shows the background-subtracted full scan

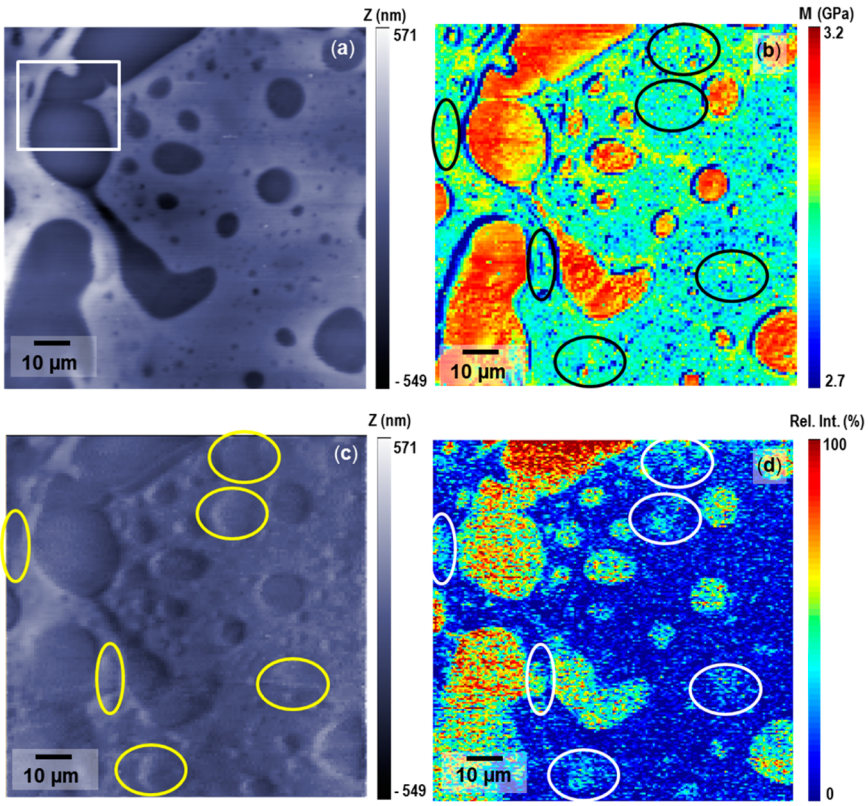

Figure 3. Co-registered AFM (a) prepyrolysis topography image, (b) BE elastic modulus image, (c) postpyrolysis topography image, and (d) mass spectrometry chemical image for *m/z* 106, obtained from an ~500 nm thick thin film of phase-separated PS/P2VP blend. The color scale for the topography goes from dark to light, which is proportional to an increase in relative surface height. Highlighted ovals in panels (b), (c), and (d) indicate areas where the AFM topography, elastic modulus, and mass spectrometry images differ in terms of the presence of P2VP. See Figure 5 for zoomed-in images of the area indicated by the white square.

averaged mass spectrum (0.07−0.15 min) obtained from Figure 2b with the signal for the protonated 2-vinylpyridine molecule at *m/z* 106 clearly visible. To confirm the identity of the observed pyrolysis products in Figure 2c, pure P2VP was directly pyrolyzed using the same heating parameters in a spot sampling mode (Figure 2d). The base peak in the spectrum was *m/z* 106 with two other much lesser abundant peaks observed at *m/z* 120 and 211, presumably corresponding to protonated 2-isopropenylpyridine and a 2-vinylpyridine dimer, respectively.[41] These other species were most likely observed in this case because of the larger area sampled and are consistent with other low-mass pyrolysis products of P2VP that have been observed using other methods of detection.[42] The mass spectrum obtained when introducing a steady headspace vapor of 2-vinylpyridine into the extractor capillary showed only the peak for the protonated 2-vinylpyridine (Figure 2e).

Co-registered Topographical, Band Excitation Nanomechanical, and Mass Spectral Imaging of a Polymer Blend. Using our hybrid AFM-TD/APCI-MS system, co-registered AFM-based topographical (Figure 3a) and BE nanomechanical elastic modulus (Figure 3b) images as well as the mass spectrometry chemical image of *m/z* 106 corresponding to 2-vinylpyridine (Figure 3c) of a 100 μm × 100 μm region of a ~500 nm thick PS/P2VP phase-separated thin film were obtained. The topographical image of the sample obtained postpyrolysis sampling is shown in Figure 3d. Data point pixel size for the topographical images was best among the three image types (390 nm × 390 nm), with the pixel size for the BE image (781 nm × 781 nm) and mass spectrometry image (690 nm × 500 nm) being comparable.

The topographic image of the sample in Figure 3a showed that there were distinct plateau and valley regions in the sample. The BE nanomechanical elastic modulus image in Figure 3b indicated that the plateau regions in the topography were, for the most part, a material distinct from the material in the valleys. This distinction was manifest by a change in the modulus of the material by ~0.3 GPa between the stiffer valleys *versus* the plateaus. The modulus values were calculated based on the change in contact resonance frequency measured across the surface as detailed in the Supporting Information. However, establishing which polymer is in which region can be more difficult using only the elastic modulus information because PS and P2VP have very similar moduli, *viz.*, around 3 GPa for bulk measurements. However, when the elastic modulus image in Figure 3b was compared to the mass spectral chemical image for 2-vinylpyridine in

Figure 3c, it was clear that the stiffer areas (~3 GPa) corresponded to P2VP. The slightly softer areas (~2.7 GPa), where no signal for P2VP was observed, must be predominately PS. Thus, the surface of the valley regions was composed of P2VP, and the surface of the plateau regions was composed of PS.

Upon close inspection of the three different images, one notes a general similarity but a few obvious differences, as highlighted by the corresponding circled regions in Figure 3b–d. We believe these differences are the effect of the inherent difference in sampling depths of the BE and the mass spectrometry pyrolysis sampling and, therefore, different data voxel size. As noted earlier, both the BE image and the mass spectrometry image have roughly the same data pixel size. In the case of BE, under ambient conditions, the sampling depth will be on the order of the probe tip radius, *viz.*, ~20 nm.[43–45] In contrast, we were able to determine under the conditions of these experiments that the TD/pyrolysis process sampled on average 110–140 nm into the surface. This was determined from line scan data (see discussion of Figure 2 above) as well as from a more quantitative imaging study (see Supplemental Figure S2). Because of this much deeper sampling depth and resulting larger voxel size, we believe the mass spectral images can represent subsurface (>20 nm in depth) chemical differences in the polymer film, such as buried interfaces, that the BE method cannot detect. Correlating features circled in the MS chemical image in Figure 3c and postpyrolysis AFM image in Figure 3d confirm the presence of these subsurface features. Methods for detecting and visualizing buried interfaces with AFM have been a growing area of study.[29]

This possibility of obtaining sometimes different information from BE and mass spectral imaging is further demonstrated by the graphical illustration in Figure 4. Figure 4a represents a polymer blend thin film with various subsurface features. Both BE and MS imaging modes coupled to AFM allow the (ambient-temperature) nano-TA probe to follow the contour of the surface. However, for BE the signal recorded results from the top 20 nm of material (blue dotted line). The heated nano-TA probe used to sample and obtain the mass spectral image also followed the surface contour but penetrates and liberates material from the sample as deep as 140 nm below the surface (yellow dotted line). At the buried interfaces labeled 1 and 2 in Figure 4a, where P2VP was buried more than 20 nm below the surface layer, signal would be observed in the mass spectrum, but not in the BE signal. Hypothetical signal levels from the line scan profiles across the surface with the two modes are shown in Figure 4b and c, respectively. BE provided information about compositional changes in the top 20 nm, revealing a higher higher elastic modulus when P2VP was at the surface, whereas mass spectral analysis was able to detect the

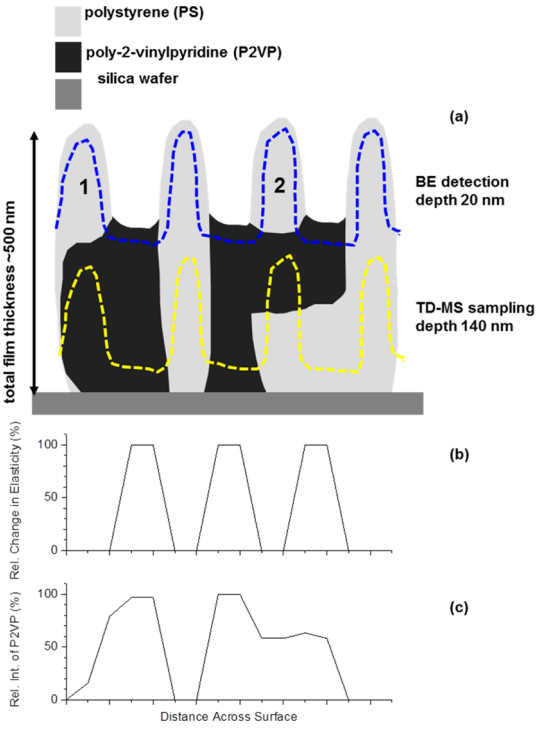

Figure 4. (a) Schematic illustration of a hypothetical phase separation of PS and P2VP inside a thin film showing the difference in the measurement depth of the AFM BE and nano-TA pyrolysis methods relative to the thickness of the film. (b) Expected AFM change in relative nanomechanical stiffness and (c) mass spectral ion signal from pyrolysis of P2VP for the line scan across the surface interface depicted in (a).

buried interface between PS and P2VP at locations 1 and 2, generating a more complex signal trace.

Achievable Mass Spectrometry Imaging Spatial Resolution. The achievable mass spectral imaging resolution was estimated to be 1.5–2.6 μm by noting some of the smallest features that were clearly resolved in the mass spectral chemical image of the polymer film as well as in the topographical and BE nanomechanical images. An example is the small elliptical-shaped P2VP valley highlighted in the zoomed regions of the various images shown in Figure 5. As determined from the topographical cross section (Figure 5d), the P2VP island was roughly 2.6 μm across in the axis parallel to the scanning direction. Some even smaller features, such as the small, ~1.6 μm sliver of PS between two domains of P2VP, were just distinguishable in all three images (area highlighted by rectangular boxes in Figure 5a–c, cross section not shown). This imaging resolution estimate was consistent with the mass spectral image data pixel size of 690 nm × 500 nm given that one might expect at least two pixels in any direction necessary to effectively define a feature.[46] The lateral resolution in the mass spectrometry images was also estimated by measuring the distance required for a rise from 20% to 80% of the signal intensity change when scanning across a PS/P2VP interface feature with a sharp edge in the film. By this 20–80% criterion,

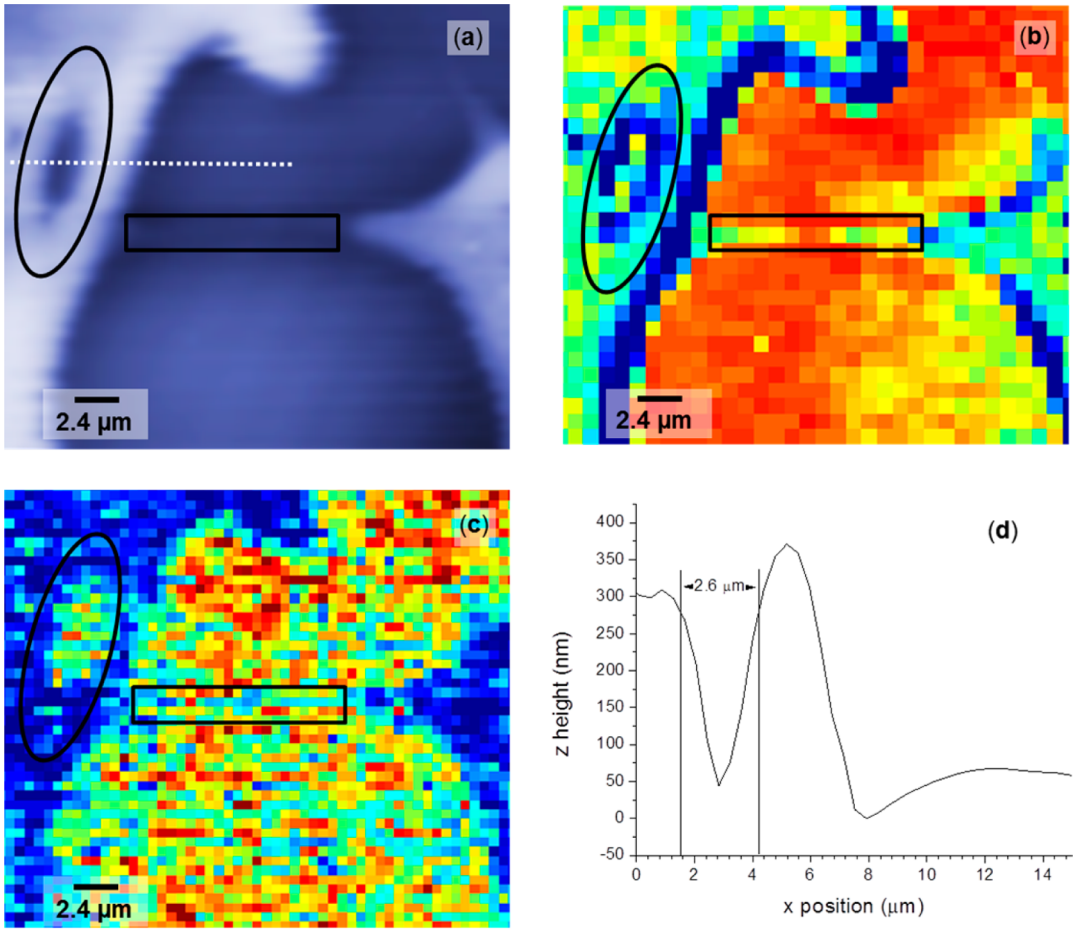

Figure 5. Zoomed-in regions of (a) AFM topography image, (b) elastic modulus image, and (c) the mass spectrometry chemical image for *m/z* 106 shown in Figure 3a, b, and d, respectively, corresponding to the area indicated by the white square in Figure 3a. Oval highlights in (a)−(c) surround an about 2.6 μm wide P2VP island distinguishable in each image (see cross section in (d) taken along the dotted line in (a)). Highlighted rectangles indicate an about 1.5 μm wide gap between P2VP features that is visible in the images in (a)−(c).

commonly used in other imaging fields, including mass spectrometry imaging,[47] the lateral resolution was estimated to be ~411 nm (Supplemental Figure S3).

CONCLUSIONS

In this paper, we reported on the development of a hybrid atmospheric pressure AFM/MS system that utilized nano-TA probes for pyrolysis surface sampling with subsequent APCI and mass spectrometric detection. This particular AFM and MS combination provided for the first time the capability to obtain on the same platform AFM-based topographical and nanomechanical images as well mass spectral-based chemical images of a sample surface. The topography image was uniquely a surface measurement, whereas the BE image was representative of the top 20 nm of the sample and the mass spectral image represented material present to a depth of 110−140 nm. Data point pixel size for the topography (390 nm × 390 nm), band excitation (781 nm × 781 nm), and mass spectrometry (690 nm × 500 nm) images was comparable, but because of the sampling depth differences, the data voxel size for each of the three images was dramatically different. For the PS/P2VP polymer sample investigated, this multimodal imaging approach provided both spatially resolved physical and chemical information as well as a means to detect chemical interfaces buried as much as 110−140 nm deep. The spatial resolution of the chemical image was estimated to be between 1.5 and 2.6 μm, based on the ability to distinguish surface features in that image that were also observed in the other images. This demonstrated chemical image resolution far exceeds other ambient chemical imaging mass spectral techniques where the best demonstrated achievable spatial resolution is on the order of 10−50 μm.[48−52] The use of a mass analyzer with faster data acquisition rates, combined with even modest improvements in detection levels, will enable significantly smaller data pixel sizes, allowing the approach to achieve submicrometer spatial resolution mass spectral images. Additionally, AFM-based topographic and nanomechanical imaging can easily achieve resolutions on the order of 10's of nanometers; therefore, data from chemical and mechanical

information channels could potentially be used to drive chemical resolution even higher through the use of data fusion.[53]

In summary, the co-registration of topographical, nanomechanical, and mass spectral images of a surface obtained by this hybrid AFM/MS instrument offers new possibilities for higher resolution characterization and detailed understanding of the surface compositions. Adding imaging capabilities such as Raman[54] or IR spectroscopy[55] would also be beneficial for material characterization, particularly in cases where surface chemical properties cannot be differentiated using a mass spectrometer, such as differentiation of an amorphous or crystalline chemical phase.

METHODS

Samples and Solvents. P2VP (M_w = 97K, M_w/M_n = 1.07, T_g = 368 K) and PS (M_w = 114K, M_w/M_n = 1.09, T_g = 368 K) were purchased from Polymer Source, Inc. (Dorval, QC, Canada) and used without further purification. Tetrahydrofuran (THF) was purchased from Sigma-Aldrich (St. Louis, MO, USA) and distilled in house to remove impurities. 2-Vinylpyridine (97%) was purchased from Sigma-Aldrich and used without further purification. Rubrene was purchased from Sigma-Aldrich and pressed into a pellet for analysis using a 13 mm diameter pellet press. Uniform coatings of yellow ink containing pigment yellow 74[56] were created by printing 1 mm wide lines of Epson yellow T0884 ink (Epson Inc., Tokyo, Japan) on ultrapremium photo paper (Epson America Inc., Long Beach, CA, USA) using an Epson Stylus NX110 inkjet printer (Epson Inc.).

Polymer Thin Film Preparation. A polymer solution was created by mixing 70 mg of PS and 70 mg of P2VP in a scintillation vial and gradually adding 1.43 g of THF to dissolve the solute until the concentration reaches ~5 wt % of each polymer. The solution was then spin coated onto a clean silicon wafer for 60 s at 7000 rpm using an EDC-650-15 spin coater (Laurell Technologies, North Wales, PA, USA). This procedure resulted in an ~500 nm thick polymer film, as measured by a Tencor P-10 profilometer (Tencor, Miliptas, CA, USA). The film was annealed in a vacuum oven at 380 K (107 °C) for 1 h. The annealing process above the glass transition temperature helped the two blended polymer phases to separate.

AFM-TD/APCI-MS System and Operation. An LTQ XL mass spectrometer (Thermo Fisher Scientific., Waltham, MA, USA) was used in this work. Material liberated from the surface by thermal desorption or pyrolysis at the AFM nano-TA probes was ionized and transferred to the mass spectrometer *via* an in-line vapor extractor/corona discharge APCI source (Figure 1). This extractor/APCI source was built within a 1/4 in. Swagelok stainless steel cross (Swagelok, Solon, OH, USA). To one arm of the cross was connected an extended version of the mass spectrometer atmosphere to vacuum transfer capillary and to the opposite arm a 4 cm long extractor capillary (1.27 mm o.d. × 0.84 mm i.d.) placed next to the AFM probe. In the upper arm was placed a stainless steel corona discharge needle (Thermo Scientific), and opposite to that was connected a nitrogen supply line from the mass spectrometer. The tip of the corona needle was positioned at the line of sight center of the cross and held in place with the Swagelok nut and an electrically isolating Teflon fitting/ferrule assembly that screwed into the extractor unit. The instrument high-voltage supply was used to initiate a corona discharge at the needle tip (constant current mode, ~0.75 μA). The auxiliary flow of nitrogen into the cross was controlled *via* a gas pressure regulator (~100 psi applied, Parker, Mayfield Heights, OH, USA) and variable leak valve (Granville-Phillips, Boulder, CO, USA). The gas flow rate into the extractor/APCI source was measured using a Matheson 602 mass flow meter (Matheson, Montgomeryville, PA, USA).

The basic AFM setup used for the experiments has been described previously.[3] Briefly, a Veeco Multimode AFM (Bruker AXS, Santa Barbara, CA, USA) equipped with a closed loop N-Point stage (N-Point, Madison, WI, USA) and a Nanonis system controller (SPECS Zurich GmbH, Zurich, Switzerland) was used for this work. The heated tips were VITA-MM-NANOTA-300 nano-TA AFM probes (Bruker AXS, Camarillo, CA, USA). The controller/power supply from an AFM+ instrument (Anasys Instruments, Santa Barbara, CA, USA) was used to supply heating voltage to the tip in power feedback mode. The position of the AFM probe tip relative to the extraction capillary was visualized for accurate positioning using a Navitar telescope with a 12× objective (Navitar Inc., Rochester, NY, USA) connected to a Costar SI-C400N CCD camera (Costar Inc., Anaheim, CA, USA). For imaging experiments, the AFM was controlled using custom software that utilized components of the Nanonis interface and in-house-developed software to turn off the heating voltage on each line scan retrace. One analog output of the Nanonis controller was used to simultaneously trigger the temperature change of the nano-TA cantilever and the mass spectrometer. Mass spectra for imaging were recorded in full scan mode with a 50 ms injection time, 5 μm/s lane scan speed, and 500 nm lane spacing.

Band excitation, as discussed in previous work,[30] was used to operate the AFM probe in a contact resonance mode.[57] In the experiment the AFM probe was excited by a digital waveform with a finite spectral density in a band centered on a resonance frequency of the probe.[30−32] The output signal was detected by a photodetector and was then Fourier transformed to produce the transfer function of the cantilever. The resulting data are a 3D data structure of $\{A, \theta\}(x, y, \omega)$, where $\{A, \theta\}$ is the response amplitude and phase, respectively, ω is the frequency, and x and y are the spatial coordinates of the measurement. For contact measurements the tip/surface system can be represented by a simple harmonic oscillator (SHO) model given by eq 1.[58]

$$H(\omega) = \frac{{A_i}^{max}{\omega_{i0}}^2 e^{i\varphi}}{\omega^2 - i\frac{\omega\omega_{i0}}{Q_i} - {\omega_{i0}}^2} \quad (1)$$

In eq 1 ${A_i}^{max}$ is the amplitude at the frequency of ith resonance, ω_{i0} is the resonance frequency, ω is the shifted frequency, φ is the phase at the frequency shift, and Q_i is the quality factor that describes energy losses in the system. Using the SHO model, 3D data were fitted to extract and plot 2D maps of SHO parameters: response amplitude, phase, resonance frequency shift, and Q-factor.

Conflict of Interest: The authors declare no competing financial interest.

Acknowledgment. The work of O.S.O., T.T., V.K., and G.J.V.B. on the fundamentals and optimization of the hybrid AFM/MS system was supported by the United States Department of Energy, Office of Science, Basic Energy Sciences, Chemical Sciences, Geosciences, and Biosciences Division. The polymer work of V.B. was supported by the U.S. Department of Energy (DOE), Office of Science, Basic Energy Sciences (BES), Materials Sciences and Engineering Division. The BE work of M.B.O., A.B., and S.J. was carried out as part of the Center for Nanophase Materials Sciences, which is a DOE Office of Science User Facility. Kevin Kjoller of Anasys Instruments is thanked for the loan of the modified AFM+ instrument.

Supporting Information Available: Supporting information describing the semiquantitative calibration of the BE contact resonance frequency shift data to elastic moduli of the material, quantitation of the amount of material removed from the surface during the pyrolysis surface sampling process, and calculation of the 80−20% resolution over a PS to P2VP domain step edge is available free of charge *via* the Internet at http://pubs.acs.org.

REFERENCES AND NOTES

1. Ovchinnikova, O. S.; Van Berkel, G. J. Thin-Layer Chromatography and Mass Spectrometry Coupled Using Proximal Probe Thermal Desorption with Electrospray or Atmospheric Pressure Chemical Ionization. *Rapid Commun. Mass Spectrom.* **2010**, *24*, 1721–1729.
2. Ovchinnikova, O. S.; Kertesz, V.; Van Berkel, G. J. Molecular Surface Sampling and Chemical Ionization Using Proximal Probe Thermal Desorption/Secondary Ionization Mass Spectrometry. *Anal. Chem.* **2011**, *83*, 598–603.
3. Ovchinnikova, O. S.; Nikiforov, M. V.; Bradshaw, J. A.; Jesse, S.; Van Berkel, G. J. Combined Atomic Force Microscope-Based Topographical Imaging and Nanometer Scale Resolved Proximal Probe Thermal Desorption/Electrospray Ionization-Mass Spectrometry. *ACS Nano* **2011**, *5*, 5526–5531.
4. Ovchinnikova, O. S.; Kjoller, K.; Hurst, G. B.; Pelletier, D. A.; Van Berkel, G. J. Atomic Force Microscope Controlled Topographical Imaging and Proximal Probe Thermal Desorption/Ionization Mass Spectrometry Imaging. *Anal. Chem.* **2014**, *86*, 1083–1090.
5. Chui, B. W.; Stowe, T. D.; Ju, Y. S.; Goodson, K. E.; Kenny, T. W.; Mamin, H. J.; Terris, B. D.; Ried, R. P. Low-Stiffness Silicon Cantilevers with Iintegrated Heaters and Piezoresistive Sensors for High-Density AFM Thermomechanical Data Storage. *J. Microelectromech. Syst.* **1998**, *7*, 69–78.
6. Price, D. M.; Reading, M.; Hammiche, A.; Pollock, H. M. Micro-Thermal Analysis: Scanning Thermal Microscopy and Localised Thermal Analysis. *Int. J. Pharm.* **1999**, *192*, 85–96.
7. Price, D. M.; Reading, M.; Hammiche, A.; Pollock, H. M. New Adventures in Thermal Analysis. *J. Therm. Anal. Calorim.* **2000**, *60*, 723–733.
8. Price, D. M.; Reading, M.; Lever, R. J.; Hammiche, A.; Pollock, H. M. Micro-Thermal Analysis of Evolved Gas Analysis. *Thermochim. Acta* **2001**, *367−368*, 195–202.
9. Price, D. M.; Reading, M.; Smith, R. M.; Pollock, H. M.; Hammiche, A. Localised Evolved Gas Analysis by Micro-Thermal Analysis. *J. Therm. Anal. Calorim.* **2001**, *64*, 309–314.
10. Reading, M.; Price, D. M.; Grandy, D. B.; Smith, R. M.; Bozec, L.; Conroy, M.; Hammiche, A.; Pollock, H. M. Micro-Thermal Analysis of Polymers: Current Capabilities and Future Prospects. *Macromol. Symp.* **2001**, *167*, 45–62.
11. Owens, S. C.; Berenbeim, J. A.; Schmidt Patterson, C.; Dillon, E. P.; de Vries, M. S. Sub-micron Proximal Probe Thermal Desorption and Laser Mass Spectrometry on Painting Cross-Sections. *Anal. Methods* **2014**, *6*, 8940–8945.
12. *Scanning Probe Microscopy of Functional Materials: Nanoscale Imaging and Spectroscopy*, 1st ed.; Kalinin, S. V.; Gruverman, A., Eds.; Springer: New York, 2011.
13. Weisenhorn, A. L.; Maivald, P.; Butt, H.-J.; Hansma, P. K. Measuring Adhesion, Attraction, and Repulsion Between Surfaces in Liquids with an Atomic-Force Microscope. *Phys. Rev. B* **1992**, *45*, 11226–11232.
14. http://www.veeco.com/pdfs/appnotes/quantitative-mechanical-property-mapping-atthe-nanoscale-with-peakforce-qnm-an128-lores.pdf.
15. Dokukin, M. E.; Sokolov, I. Quantitative Mapping of the Elastic Modulus of Soft Materials with HarmoniX and Peak Force QNM AFM Modes. *Langmuir* **2012**, *28*, 16060–16071.
16. Sahin, O.; Magonov, S.; Su, C.; Quate, C. F.; Solgaard, O. An Atomic Force Microscope Tip Designed to Measure Time-Varying Nanomechanical Forces. *Nat. Nanotechnol.* **2007**, *2*, 507–514.
17. Rosa-Zeiser, A.; Weilandt, E.; Hild, S.; Marti, O. The Simultaneous Measurement of Elastic, Electrostatic and Adhesive Properties by Scanning Force Microscopy: Pulsed-Force Mode Operation. *Meas. Sci. Technol.* **1997**, *8*, 1333–1338.
18. http://www.anasysinstruments.com/products/thermal-probes-tips-afm-sthm/.
19. Gannepalli, A.; Yablon, D. G.; Tsou, A. H.; Proksch, R. Mapping Nanoscale Elasticity and Dissipation Using Dual Frequency Contact Resonance AFM. *Nanotechnology* **2011**, *22*, 355705.
20. http://www.anasysinstruments.com/technology/lcr/.
21. https://www.asylumresearch.com/Products/iDrive/iDrive.shtml.
22. Fleming, Y.; Wirtz, T.; Gysin, U.; Glatzel, T.; Wegmann, U.; Meyer, E.; Maier, U.; Rychen, J. Three Dimensional Imaging Using Secondary Ion Mass Spectrometry and Atomic Force Microscopy. *Appl. Surf. Sci.* **2011**, 1322–1327.
23. Bernard, L.; Heier, J.; Paul, W.; Hug, H. J. The SFM/ToF-SIMS Combination for Advanced Chemically-Resolved Analysis at the Nanoscale. *Nucl. Instrum. Methods Phys. Res., Sect. B* **2014**, *339*, 85–90.
24. Nudnova, M. N.; Sigg, J.; Wallimann, P.; Zenobi, R. Plasma Ionization Source for Atmospheric Pressure Mass Spectrometry Imaging Using Near-Field Optical Laser Ablation. *Anal. Chem.* **2015**, *87*, 1323–1329.
25. National Research Council. *Visualizing Chemistry: The Progress and Promise of Advanced Chemical Imaging*; The National Academies Press: Washington, DC, 2006.
26. Moreno-Flores, S.; Toca-Herrera, J. L. The New Future of Scanning Probe Microscopy: Combining Atomic Force Microscopy with Other Surface-Sensitive Techniques, Optical Microscopy and Fluorescence Techniques. *Nanoscale* **2009**, *1*, 40–49.
27. Petibois, C. Imaging Methods for Elemental, Chemical, Molecular, and Morphological Analyses of Single Cells. *Anal. Bioanal. Chem.* **2010**, *397*, 2051–2065.
28. Masyuko, R.; Lanni, E. J.; Sweedler, J. V.; Bohn, P. W. Correlated Imaging – A Grand Challenge in Chemical Analysis. *Analyst* **2013**, *138*, 1924–1939.
29. Ebeling, D.; Eslami, B.; Solares, S. D. Visualizing the Subsurface of Soft Matter: Simultaneous Topographical Imaging, Depth Modulation, and Compositional Mapping with Triple Frequency Atomic Force Microscopy. *ACS Nano* **2013**, *7*, 10387–10396.
30. Jesse, S.; Kalinin, S. V.; Proksch, R.; Baddorf, A. P.; Rodriguez, B. J. The Band Excitation Method in Scanning Probe Microscopy for Rapid Mapping of Energy Dissipation on the Nanoscale. *Nanotechnology* **2007**, *18*, 435503.
31. Kalinin, S. V.; Rodriguez, B. J.; Jesse, S.; Proksch, R. A Biased View of the Nanoworld: Electromechanical Imaging by SPM. *R&D Mag.* **2007**, *49*, 34–36.
32. Jesse, S.; Vasudevan, R. K.; Collins, L.; Strelcov, E.; Okatan, M. B.; Belianinov, A.; Baddorf, A. P.; Proksch, R.; Kalinin, S. V. Band Excitation in Scanning Probe Microscopy: Recognition and Functional Imaging. *Annu. Rev. Phys. Chem.* **2014**, *65*, 519–536.
33. Takahashi, Y.; Ochiai, N.; Matsushita, Y.; Noda, I. Viscoelastic Properties of Poly(2-vinylpyridine) in Bulk and Solution. *Polym. J.* **1996**, *28*, 1065–1070.
34. Gunton, J. D.; San Miguel, M.; Sahni, P. S. The Dynamics of First Order Phase Transitions. In *Phase Transitions and Critical Phenomena*; Domb, C., Lebovitz, J. L., Eds.; Academic Press: New York, 1983; Vol. 8, pp 269−466.
35. Binder, K. Spinodal Decomposition. In *Materials Science and Technology*; Haasen, P., Ed.; VCH-Verlag: Weinheim, 1990. Vol. 5, pp 405−471.
36. Krausch, G. Surface Induced Self-Assembly in Thin Polymer Films. *Mater. Sci. Eng.* **1995**, *14*, 1–94.
37. Walheim, S.; Ramstein, M.; Steiner, U. Morphologies in Ternary Polymer Blends after Spin-Coating. *Langmuir* **1999**, *15*, 4828–4836.
38. Xue, J. Perspectives on Organic Photovoltaics. *Polym. Rev.* **2010**, *50*, 411–419.
39. Klee, S.; Derpmann, V.; Wiβdorf, W.; Klopotowski, S.; Kersten, H.; Brockmann, K. J.; Benter, T.; Albrecht, S.; Bruins, A. P.; Dousty, F.; *et al.* Are Clusters Important in Understanding the Mechanisms in Atmospheric Pressure Ionization? Part 1: Reagent Ion Generation and Chemical Control of Ion Populations. *J. Am. Soc. Mass Spectrom.* **2014**, *25*, 1310–1321.
40. Moini, M. Atmospheric Pressure Chemical ionization: Principles, Instrumentation and Applications. In *The Encyclopedia of Mass Spectrometry, Vol. 6, Ionization Methods*; Gross, M. L.; Caprioli, R. M., Eds.; Elsevier: New York, NY, 2007; pp 344−354.

41. Elmaci, A. Thermal Characterization of Homopolymers, Copolymers and Metal Functional Copolymers of Vinylpyridines. Masters Thesis, Middle East Technical University, 1998.
42. Ohtani, H.; Kotsuji, H.; Momose, H.; Matsushita, Y.; Noda, I.; Tsuge, S. Ring Structure of Cyclic Poly(2-vinylpyridine) Proved by Pyrolysis. *Macromolecules* **1999**, *32*, 6541–6544.
43. Tsong, T. T. Field Penetration and Band Bending near Semiconductor Surfaces in High Electric Fields. *Surf. Sci.* **1979**, *81*, 28–42.
44. Sarioglu, A. F.; Atalar, A.; Degertekin, F. L. Modeling the Effect of Subsurface Interface Defects on Contact Stiffness for Ultrasonic Atomic Force Microscopy. *Appl. Phys. Lett.* **2004**, *84*, 5368–5370.
45. Crozier, K. B.; Yaralioglu, G. G.; Degertekin, F. L.; Adams, J. D.; Minne, S. C.; Quate, C. F. Thin Film Characterization by Atomic Force Microscopy at Ultrasonic Frequencies. *Appl. Phys. Lett.* **2000**, *76*, 1950–1952.
46. Jerri, A. J. The Shannon Sampling Theorem— Its Various Extensions and Applications: A Tutorial Review. *Proc. IEEE* **1977**, *65*, 1565–1596.
47. Colliver, T. L.; Brummel, C. L.; Pacholski, M. L.; Swanek, F. D.; Ewing, A. G.; Winograd, N. Atomic and Molecular Imaging at the Single-Cell Level with TOF-SIMS. *Anal. Chem.* **1997**, *69*, 2225–2231.
48. Laskin, J.; Heath, B. S.; Roach, P. J.; Cazares, L.; Semes, O. J. Tissue Imaging Using Nanospray Desorption Electrospray Ionization Mass Spectrometry. *Anal. Chem.* **2012**, *84*, 141–148.
49. Lorenz, M.; Ovchinnikova, O. S.; Kertesz, V.; Van Berkel, G. J. Laser Microdissection and Atmospheric Pressure Chemical Ionization Mass Spectrometry Coupled for Multimodal Imaging. *Rapid Commun. Mass Spectrom.* **2013**, *27*, 1429–1436.
50. Robichaud, G.; Barry, J. A.; Garrard, K. P.; Muddiman, D. C. Infrared Matrix-Assisted Laser Desorption Electrospray Ionization (IR-MALDESI) Imaging Source Coupled to a FT-ICR Mass Spectrometer. *J. Am. Soc. Mass Spectrom.* **2013**, *24*, 92–100.
51. Ovchinnikova, O. S.; Bhandari, D.; Lorenz, M.; Van Berkel, G. J. Transmission Geometry Laser Ablation into a Non-Contact Liquid Vortex Capture Probe for Mass Spectrometry Imaging. *Rapid Commun. Mass Spectrom.* **2014**, *28*, 1665–1673.
52. Chen, L. C.; Yosimura, K.; Yu, Z.; Iwata, R.; Ito, H.; Suzuki, H.; Mori, K.; Ariyada, O.; Takeda, S.; Kubota, T.; *et al*. Ambient Imaging Mass Spectrometry by Electrospray Ionization Using Solid Needle as Sampling Probe. *J. Mass Spectrom.* **2009**, *44*, 1469–1477.
53. Tarolli, J. G.; Jackson, L. M.; Winograd, N. Improving Secondary Ion Mass Spectrometry Image Quality with Image Fusion. *J. Am. Soc. Mass Spectrom.* **2014**, *25*, 2154–2162.
54. Stockle, R. M.; Suh, Y. D.; Deckert, V.; Zenobi, R. Nanoscale Chemical Analysis by Tip-Enhanced Raman Spectroscopy. *Chem. Phys. Lett.* **2000**, *318*, 131–136.
55. Dazzi, A.; Prater, C. B.; Hu, Q.; Chase, D. B.; Rabolt, J. F.; Marcott, C. AFM-IR: Combining Atomic Force Microscopy and Infrared Spectroscopy for Nanoscale Chemical Characterization. *Appl. Spectrosc.* **2012**, *66*, 1365–1384.
56. Donnelly, S.; Marrero, J. E.; Cornell, T.; Fowler, K.; Allison, J. Analysis of Pigmented Inkjet Printer Inks and Printed Documents by Laser Desorption/Mass Spectrometry. *J. Forensic Sci.* **2010**, *55*, 129–135.
57. Nikiforov, M. P.; Gam, S.; Jesse, S.; Composto, R. J.; Kalinin, S. V. Morphology Mapping of Phase-Separated Polymer Films Using Nanothermal Analysis. *Macromolecules* **2010**, *43*, 6724–6730.
58. Garcia, R.; Perez, R. Dynamic Atomic Force Microscopy Methods. *Surf. Sci. Rep.* **2002**, *47*, 197–301.